Probing molecular dynamics using pulsed nuclear magnetic resonance

Roshan Chacko
Supervisor: Alexey Potapov

University of Nottingham
School of Physics and Astronomy

May 2021

Abstract

A bench-top NMR spectrometer based on the Red Pitaya microcomputer was used to probe the molecular dynamics of 6 alcohol samples by obtaining their $T1$ and $T2$ values. The pulse sequences used to obtain those values were the single echo spin echo pulse and the inversion recovery pulse, respectively. The samples used were methanol, propan-1-ol, glycerol, butan-1-ol, pentan-3-ol and decan-1-ol. The $T1$ times recorded were respectively 2460 ± 150 ms, 1542 ± 26 ms, 65 ± 2 ms, 1176 ± 72 ms, 603 ± 17 ms and 343 ± 4 ms. The T2 times recorded were respectively 58 ± 10 ms, 39 ± 8 ms, 42 ± 1 ms, 28 ± 3 ms, 15 ± 2 ms and 9 ± 1 ms. It was noticed that as the carbon chain length increased, both $T1$ and $T2$ decreased in an exponential manner. Glycerol had the lowest $T1$ time however, and as seen, this was due to it molecular structure instead of the carbon chain length. The report briefly touches on correlation time and its relation to the results obtained above, and the room for improvement for this experiment.

Contents

1 Introduction

The roaring 20s marked an important milestone for the foundations of quantum physics. Otto Stern had conceptualised an experiment to investigate the quantisation of angular momentum in 1922[3], and a year later, this was realised by Walther Gerlach as the infamous Stern-Gerlach experiment. The experiment was proof of the property of 'spin' – where the results showed that particles possess intrinsic angular momentum, allowing us to treat them as classical magnets using this property. The magnetic aspect that arises from spin can be characterised by the magnetic moment vector, μ.

In 1938, Isidor Rabi extended the Stern-Gerlach experiment using molecular beams travelling through a magnetic field[8]. Rabi had used the precession of the spins of the molecules to calculate the magnetic moment directly with high precision. The term he coined to describe this phenomena was called **nuclear magnetic resonance** or **NMR**.

However, the experiment by Rabi was 'unnatural' compared to today's standards of NMR experiments. The molecular beams needed to be in a vacuum, making the experiment less accessible.

Fortunately, seven years later after Rabi's success, two independent teams led by Felix Bloch[1] and Edward Purcell[7] expanded Rabi's experiment to work with condensed matter, where they exhibited the NMR phenomenon in water and paraffin, respectively. Purcell's team used the method of measuring the radiation absorption while slowly increasing the external magnetic field, whereas Bloch used the method of detecting a 'nuclear induction' signal by using a receiver coil around his water sample in his apparatus.

While Purcell's method of energy absorption was quantum mechanical in nature and Bloch's method of nuclear induction was classical in nature, both experiments yielded verifiable results matching the predicted NMR phenomenon of hydrogen nuclei. In addition to this, both Bloch and Purcell used a continuous wave (CW) of a constant frequency of EM radiation to irradiate their samples as they swept through the magnetic field through the resonance condition.

In his paper, Bloch further suggested using radio frequency (RF) pulses to induce NMR. In 1950, Erwin Hahn demonstrated this[4] – and this technique is called pulsed NMR. Nowadays, pulsed NMR is more popular than CW NMR. Hahn extended his experiment to show that multiple RF pulses preserved the NMR signal for longer, leading to the technique known as spin-echo NMR.

In this experiment, we use the spin-echo technique and another technique called recovery inversion to study the molecular dynamics of 6 samples of alcohol. Each sample has 2 characteristic times, known as $T1$ and $T2$ times, which we obtain through the manipulation of our NMR data.

2 Theory

2.1 Nuclear spin and precession

NMR is the phenomena experienced by the nuclei of certain atoms when immersed in a static magnetic field whilst exposed to a second oscillating magnetic field. NMR only works with atoms that have an odd number of protons or an odd number of neutrons. The reason for this is to ensure that the sample containing those nuclei have nuclei with a non-zero nuclear spin. This is the case with the hydrogen (^{1}H) atom. Since most organic molecules have the ^{1}H atom, NMR is an effective tool to probe them.

The nuclear spin quantum number, I, has a corresponding spin angular momentum L and contains a set of quantized spin states. The magnitude of the spin angular momentum is given by:

$$L = \hbar\sqrt{I(I+1)} \tag{1}$$

where $\hbar$ is the reduced Planck's constant.

The nucleus has an inherent charge and a spinning charge generates a magnetic field. Using this idea, we can get an expression for the magnitude of the magnetic moment, μ:

$$\mu = \gamma L \tag{2}$$

where γ is a constant called the gyromagnetic ratio. The gyromagnetic ratio is determined empirically and is unique for each nucleus type. The concept of the nuclear magnetic moment allows us to treat nuclei as tiny bar magnets.

In a sample we have multiple nuclei, and as such, the magnetic moments of the nuclei are randomly oriented in the absence of an external magnetic field.

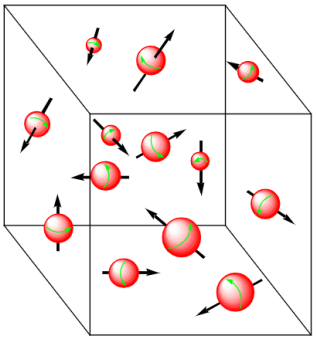

Figure 1: The random orientations magnetic moments in the absence of an external magnetic field. Image adapted from `https://health.uconn.edu/bioinformatics/wp-content/uploads/sites/162/2017/11/NMRBasics_2016.pdf`

When an external magnetic field, B_0, is applied, the spins start aligning themselves in the direction of the B_0, as bar magnets would. However, the external magnetic field also exerts a torque on the nuclear angular momentum, L, which we saw earlier arises from the spin of the nucleus. This causes the precession of the spins (this phenomenon is called **nuclear precession**)

as they align themselves, and is caused by the conservation of angular momentum - analogous to the precession of a spinning top. This precession has a frequency, ω, called the **Larmor frequency**, and is given by:

$$\omega = \gamma B_0 \tag{3}$$

The alignments of the spins are quantized, where the number of "spin states" is given by $2I + I$. For the sake of NMR, we can characterise nuclei spin with a 2-level system with spin states $+\frac{1}{2}$ and $-\frac{1}{2}$. The particle can transition between the 2 energy states by the absorption of the photon, provided that the energy of the photon, E, matches the the energy difference between the 2 states:

$$E = \hbar\gamma B = \hbar\omega \tag{4}$$

2.2 Relaxation theory

In the previous subsection, we saw that applying an external magnetic field causes the nuclear precession of spins. This question now arises - how can we know what fraction of the population of spins is aligned anti-parallel ($-\frac{1}{2}$ spin) and what fraction is aligned parallel ($\frac{1}{2}$ spin)? In thermal equilibrium, we can use this Boltzmann distribution:

$$\frac{N_-}{N_+} = \exp\left(-\frac{\Delta E}{k_B T}\right) \tag{5}$$

where N_- is the number of anti-parallel alignments, N_+ is the number of parallel alignments, ΔE is the energy difference stated in equation 4, k_B is Boltzmann's constant and T is temperature in Kelvin. From this equation, we can see that at higher temperatures, we get more anti-parallel alignments than parallel alignments.

To make the problem of multiple spins a lot simpler, we introduce the net magnetisation, M_0, which is the sum of all the individual spins (see figure below).

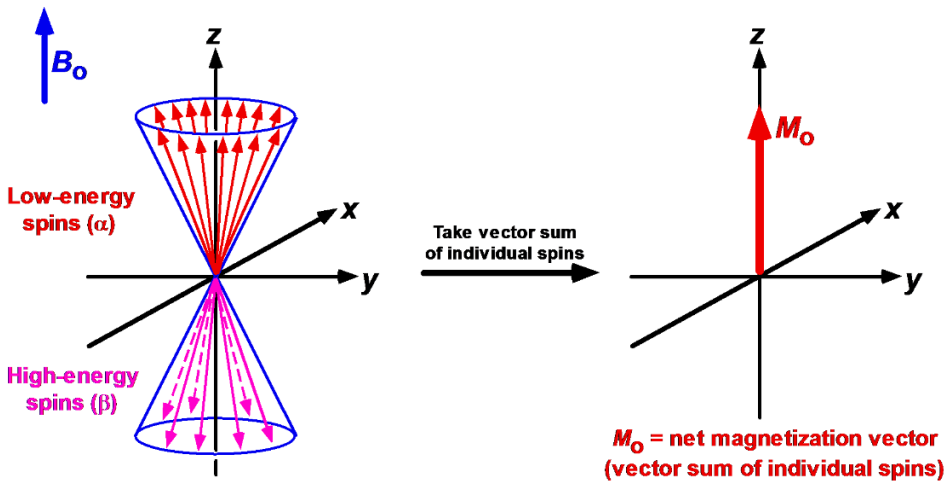

Figure 2: M_0 is the net magnetisation, which is the vector sum of the individual spins. Image adapted from `https://health.uconn.edu/bioinformatics/wp-content/uploads/sites/162/2017/11/NMRBasics_2016.pdf`

Nuclear precession is only one part of the story. Is there a way of exciting the lower energy spins to the higher energy state without increasing the temperature? The answer is by using radio-frequency (RF) excitation. We know that the energy of this RF excitation is given in equation 4. Thus, Excitation in turn also increases M_0.

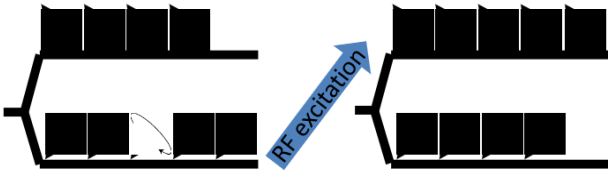

Figure 3: Pictorial description of excitation of spin state via RF radiation. Image adapted from `https://health.uconn.edu/bioinformatics/wp-content/uploads/sites/162/2017/11/NMRBasics_2016.pdf`

Excitation also allows us to change the orientation of the M_0 vector. When the RF pulse is applied in the transverse plane, it will nutate the M_0 vector by a certain angle θ, and is expressed by:

$$\theta = \gamma B_1 t_p \tag{6}$$

where B_1 is the strength of RF pulse and t_p is the duration of RF pulse. In NMR experiments we generally use 90° and 180° pulses.

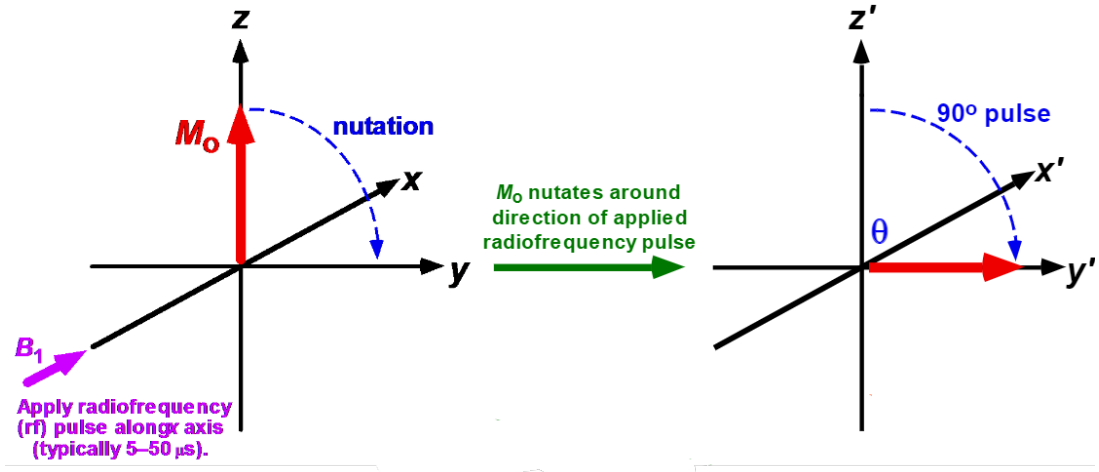

Figure 4: The nutation of M_0 due to a 90° RF pulse. We can control the degree to which M_0 is flipped by using equation 6. Image adapted from `https://health.uconn.edu/bioinformatics/wp-content/uploads/sites/162/2017/11/NMRBasics_2016.pdf`

After the excitation, the spins go through a process called **relaxation**. Relaxation is how the net magnetisation, M_0, from the spins reaches its equilibrium value. We can analyse the equilibrium M_0 with its vector components in the x (M_x), y (M_y) and z (M_z) directions. The convention is that B_0 is in the z-direction, and so M_z is non zero in equilibrium, whereas M_x and M_y (also known as the transverse plane) are zero in equilibrium.

Thus, the process by which M_z returns to its equilibrium is called **longitudinal relaxation**, and the process by which the transverse magnetisation (M_x and M_y) reaches the equilibrium value of zero is called **transverse relaxation**. We can represent these 2 types of relaxation mathematically with an exponential relation, yielding the time constants we saw earlier in the introduction - $T1$ and $T2$. For longitudinal relaxation, we have

$$M_z(t) = M_0 \left(1 - \exp \frac{-t}{T1}\right) \tag{7}$$

and for transverse relaxation we have

$$M_x(t) = M_0 \left(\exp \frac{-t}{T2}\right) \sin \omega t \tag{8}$$

$$M_y(t) = M_0 \left(\exp \frac{-t}{T2}\right) \cos \omega t \tag{9}$$

The above equations are solutions after a 90° pulse to a set of differential equations known as the Bloch equations.

Relaxation is a slow process compared to other molecular and atomic processes. The excited electronic state has a lifetime of a few microseconds and rotational energies have lifetimes of a few nanoseconds. In contrast, the relaxation process spans between milliseconds to seconds till equilibrium is reached. The advantage of slow relaxation is that transverse magnetisation (along the $x - y$ plane) survives long enough to be manipulated/observed. The disadvantage is that fewer repeats can be made, which can stop us from improving the signal-to-noise ratio of our NMR signal.

2.3 Multiple pulse sequences

Previously, we saw that we can change the alignment of M_0 by varying the characteristics of our pulse, and we saw that relaxation was an exponential decay. This decay is known as a **free induction decay** or **FID** signal, and is shown in the figure below.

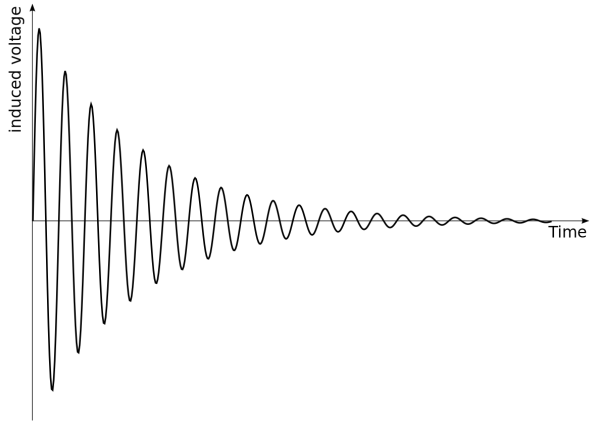

Figure 5: Free induction decay signal after an RF pulse on the sample. Image adapted from `https://en.wikipedia.org/wiki/Free_induction_decay`

How do we get the $T1$ and $T2$ times from this signal? The answer is by using multiple pulses. We will first look at the single echo spin echo sequence.

2.3.1 Spin Echo pulse sequence

A **spin-echo pulse sequence** consists of a 90° pulse and then a 180° pulse, which causes an echo in the signal. Below is an example of that signal:

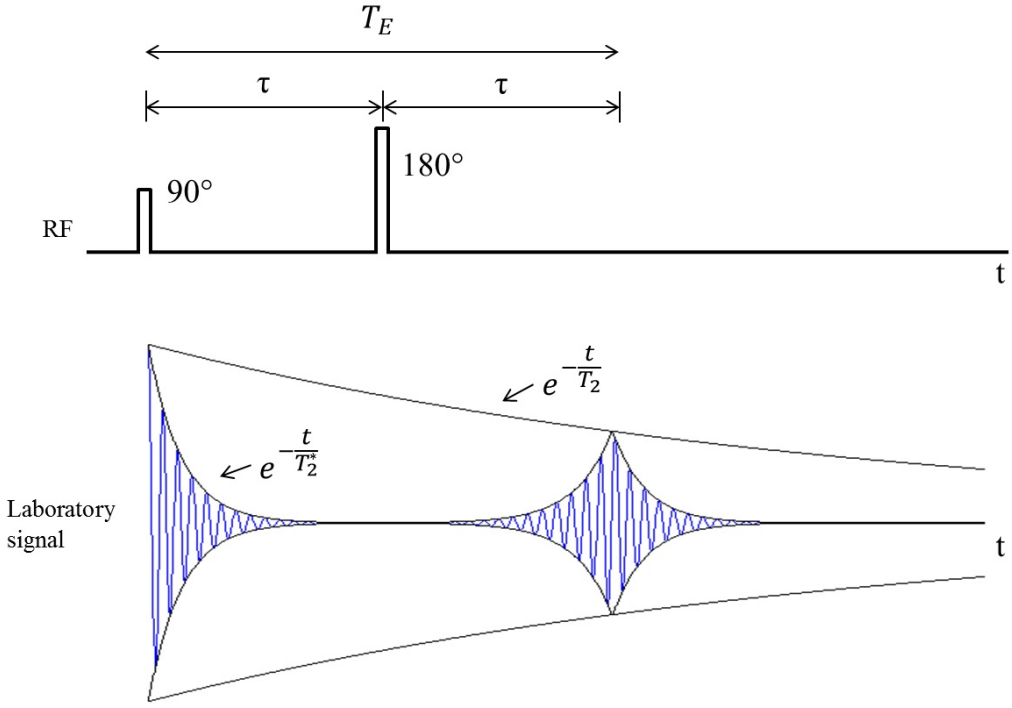

Figure 6: Above, you can see the 90° pulse and the 180° pulse sequence. Below, you can see the echo that happens a time τ after the 180° pulse, which is the same time between the pulses. Image adapted from `http://193.224.48.74/tiki-index.php?page=Spin+Echo`

From the figure above, we can see that the second pulse allows us to calculate the $T2$ time from the FID. We also see a $T2*$ time, which is known as the observed $T2$ time, which factors in the magnetic field inhomogeneities. We do not need to know that for the sake of this report. The time between the 90° pulse and the echo is known as the echo time, T_E, which is just 2τ. T_E is an important value, and it will used in this experiment to determine the $T2$ value for our alcohol samples.

We can understand why the spin-echo technique works in obtaining the $T2$ time with a nanoscale picture. Figure 7 shows directions of the spins through the progression of the pulse sequence. The 90° pulse nutates the spins as shown in 7B. Between the 90° pulse and the 180° pulse, the spins dephase. This is due to local microscopic fields that cause some spins to gain phase relative to others. When the 180° pulse is applied, it flips the spins, allowing the slower spins to 'catch up' and come into phase, eventually causing the 'echo, as shown in 7F.

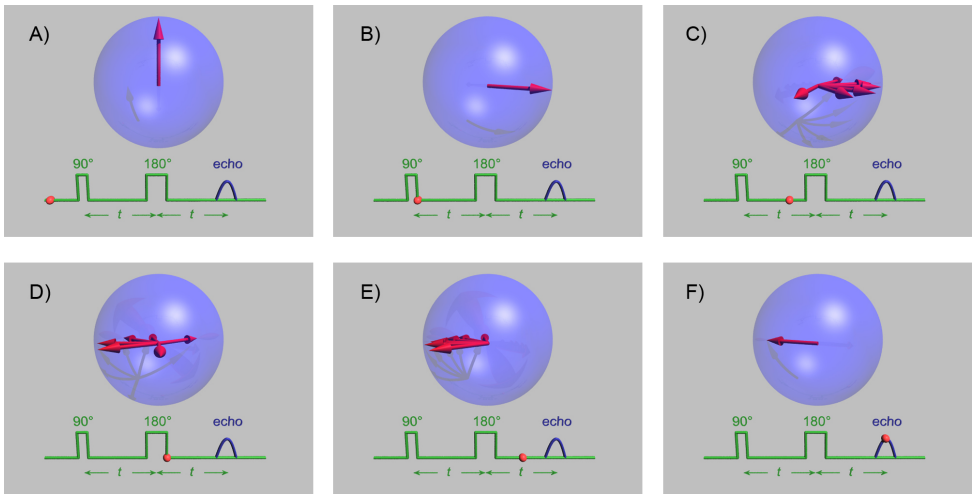

Figure 7: The directions of spins with the progression of the spin-echo pulse sequence. The red dot on the pulse diagram shows the stage of the pulse sequence. Image adapted from the animation in `http://mriquestions.com/spin-echo1.html`

2.3.2 Inversion recovery pulse sequence

To obtain a $T1$ time from our signal, we use the **inversion recovery pulse sequence**. The sequence starts with a 180° pulse followed by a 90° pulse, followed once again by a 180° pulse which then causes an echo. The purpose of the first 180° pulse is to invert M_0. The time between the 180° pulse and the 90° pulse is known as the inversion time, T_I, and is the time we use to determine $T1$ experimentally. During T_I, the spins seek to re-establish M_0 along the $+z$ axis, which are then aided by the 90° pulse to cause the echo after the 180° pulse.

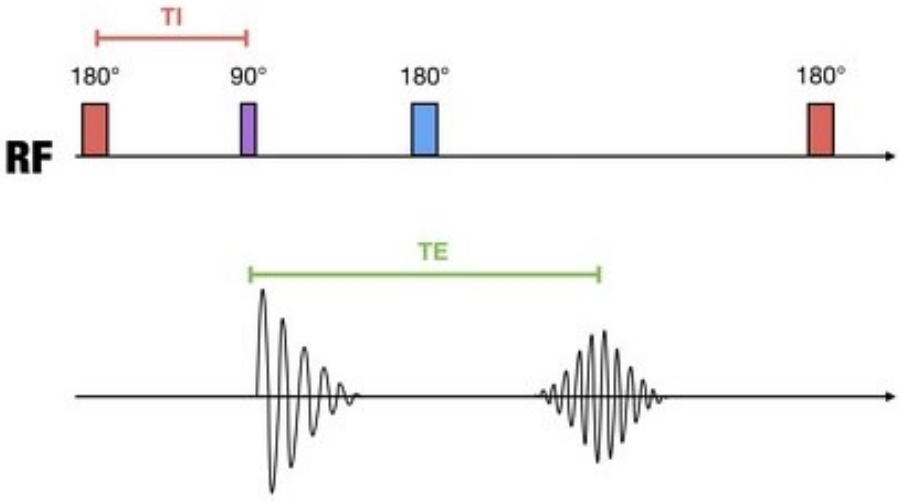

Figure 8: The inversion recovery pulse sequence. T_E is the echo time, as seen in the spin-echo pulse sequence. Image adapted from `https://radiopaedia.org/`

3 Methods

3.1 NMR apparatus setup

The apparatus used for the experiment was designed and built by Peter Yeo and Karanjit Manak [6] at the University of Nottingham. The magnet used for the experiment is an 18.45 MHz (0.43 T) electromagnet cooled by a water cooling system. A brief signal flow diagram of the NMR setup is given below:

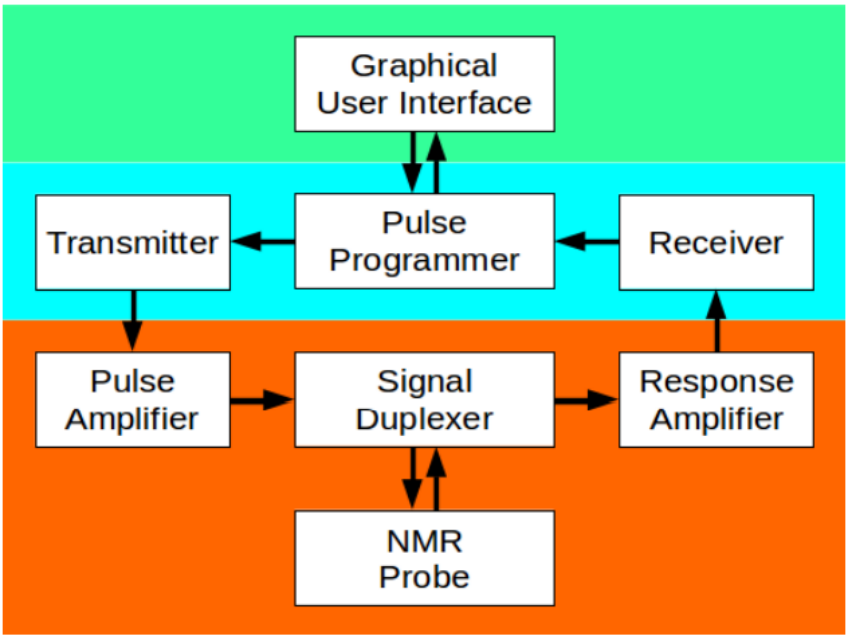

Figure 9: Signal flow diagram of the bench top NMR setup. It's implementation involves a computer (green area), a Red Pitaya (blue) and its external circuitry (orange)

The data acquisition (DAQ) interface used to receive signals from the NMR coil is called the Red Pitaya, which has both an analogue-to-digital converter (ADC) and a digital-to-analogue converter (DAC), allowing the communication between the Python code which controls the NMR coil settings and outputs the signal, and the coil containing the sample.

To understand this setup, and to understand why we use this setup, we need to start at the small coil that is wrapped around the sample in the test tube. This coil is used both as an RF transmitter to produce RF pulses and as a receiver of the NMR signal from the probe.

The RF pulses in pulsed NMR is in the order of a 100 W, while the NMR signal from the probe is in the order of a few μV. It is for this reason that we need to be careful about the sensitivity of the coil.

This is why we introduce the 'duplexer'. The duplexer is like a fast acting switch - when the pulse is on, the high power RF is routed to the probe, and input to the receiver is disconnected. When the pulse is off, the receiver is connected to the probe and the transmitter is disconnected.

This is the overall picture of the signal flow: The Python code on the computer allows us to change the frequency and the pulse settings. We then output the settings, and the Red Pitaya

converts this to an analogue signal. The signal then gets amplified by the amp and then goes through the duplexer and then through the coil to provide the RF pulse.

The relaxation is then received by the coil and then goes through the duplexer into the amp for the amplified signal, and then the Red Pitaya converts it to a digital signal and then the Python program displays it in the interface. The Python GUI is shown in the figure below:

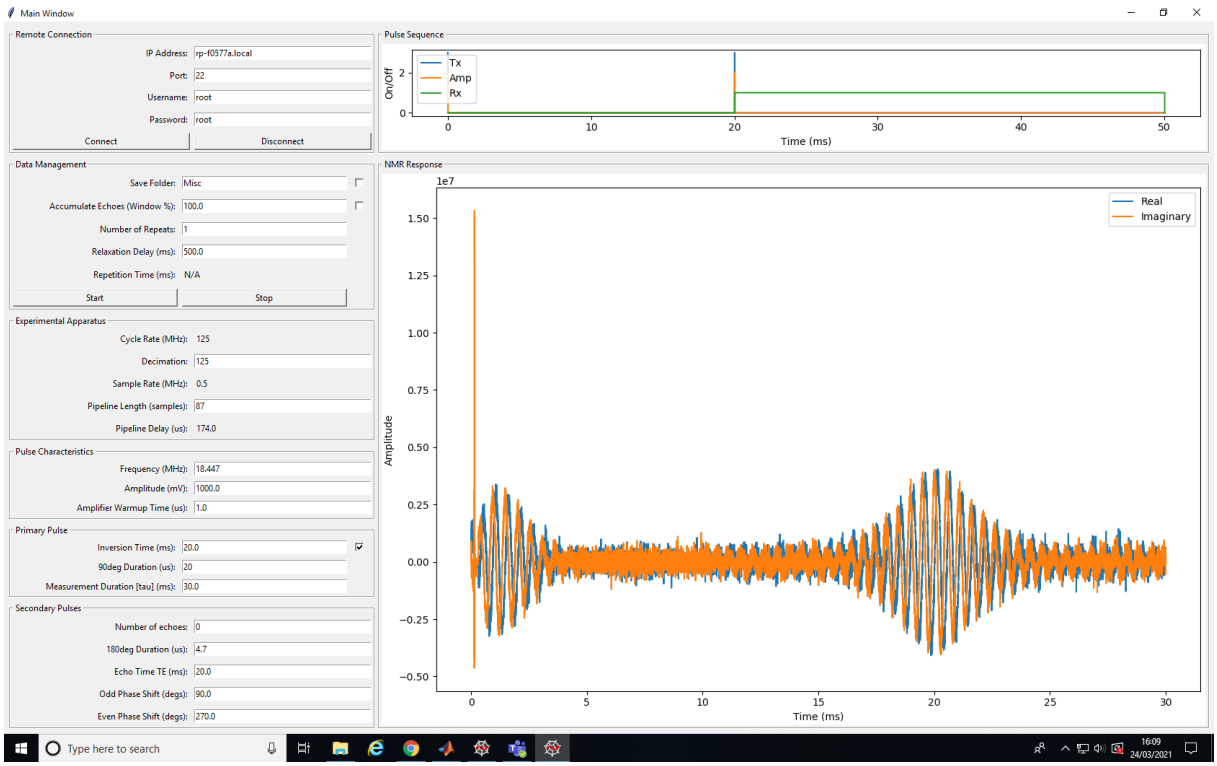

Figure 10: Python GUI used to control the NMR machine.

3.2 Sample setup

To prepare the sample in a test-tube, we had to first wash the test-tube and dry it with acetone. We then put a couple of drops of the alcohol sample in the test-tube and then put a rubber stopper around the neck of the test-tube. This was to ensure that the sample would be at the right level in the NMR machine so that the probe could record the NMR signals precisely. In addition to this, we had to ensure that only a few drops of the sample were used, so that the magnetisation would affect the whole sample and not just the lower part of the sample, which would reduce the precision of the results leading to systematic errors. Thus, we used 3-5 drops of sample using a pipette.

3.3 Obtaining NMR signals

After generating the GUI and establishing connection between the computer and the Red Pitaya, we need to find the resonant frequency needed for each sample within the lab environment. Different frequencies were used as the temperature of the room varied during the day. In addition, some measurements were done before the Easter break, where the weather was much cooler

compared to lab environment after the break. This varied the resonant frequency by a few kHz before and after the break for the samples. The resonant frequency for each sample can be found in the next section.

For the inversion recovery experiment, we needed to check the 'Inversion Time' field in the GUI and input the inversion time we needed. The range of inversion times depended on the sample - for short $T1$ times we used a smaller range of times and vice versa. Realistically, I took readings till $T_I = 1000$ ms and then plotted the results to see if the curve was sufficient to get exponential coefficient. If not, then I continued taking values till $T_I = 3000$ ms.

For the spin echo experiment, the procedure was the same as with the inversion experiment, however, here we needed to input the echo time, T_E. The GUI provided the option to have multiple pulses, but for the sake of this experiment, we used just one pulse sequence. The range of echo times used were from 10 to 180 ms.

I did 4 repeats for each measurement for both the spin-echo and inversion experiments, and then discarded the first FID signal. I noticed that the first reading increased the size of the error bars. The error bars were calculated by the standard deviation of the 3 repeats.

3.4 Processing NMR signals

The signal data saved from the Python program can be opened via a text editor, but it doesn't make a lot of sense since it is in Unicode encoding. Legacy MATLAB code was provided to read the data and to process it. After reading the data, the program omitted a couple of points (90 points is the default value) at the beginning so that any voltage spikes weren't recorded at the beginning. We then need to map our data, which currently is in the time domain, to the frequency domain. The reason for doing so is that the data of the population of spins aligned is stored in the frequency domain. We do this by taking a fourier transform (FT) of the data. The algorithm used by the program is known as the fast Fourier transform (FFT).

After taking the FFT of the signal, we then choose a region around the maximum of the FFT and then find the area under the curve for that region using the `trapz` function in MATLAB. The area under the FFT gives us the intensity, which directly correlates to the population of spins aligned. We then plot the area under the curve vs. the inversion time to get our T1 curve, and area under the curve vs. the echo time to get our T2 curve. Finally, to get our $T1$ and $T2$ values, we use an exponential curve fitting via the curve fitting tool in MATLAB. The fitting functions used are mentioned in the next section.

4 Results

4.1 $T1$

For all of my inversion recovery measurements, I used a measurement window of 30 ms. Due to this, taking $T1$ measurements was quite slow due to the buffer limit of the Red Pitaya. Moreover, since I only used one inversion recovery pulse sequence (as opposed to multiple pulse sequences), the measurement window of 30 ms was sufficient.

To make the analysis easier, I scaled down the area under the Fourier transform peak by 10^8 to 10^{10} (it varied with each sample), so the results you see below are the scaled down areas. It doesn't matter how much we scale it down by since the only value we need is the $T1$ value which is the term in the exponential function. The general fitting function used for this set of data was

$$-a\exp(-x/b)+c \tag{10}$$

The fitted value of b yielded our $T1$ value for the sample.

4.1.1 Methanol

Below is the area under FT peak vs. the inversion time for methanol.

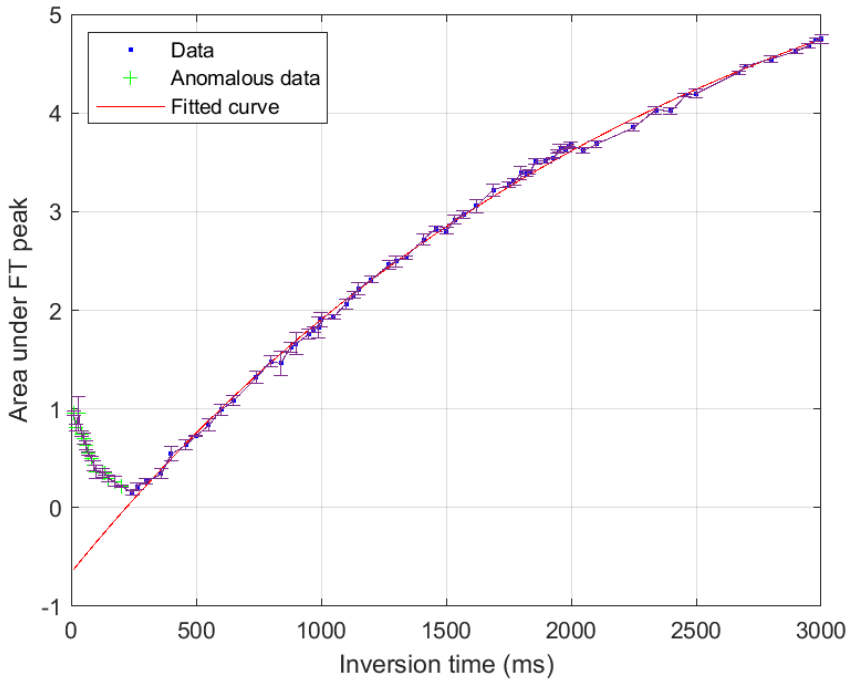

Figure 11: Area under Fourier Transform of the FID peak vs. the inversion time for methanol. The $T1$ time obtained after curve-fitting was 2460.06 ± 153.21 ms (95% confidence bounds)

From the graph we can see that the first few values till the 265 ms point were omitted as anomalous for the fitted curve. To understand why this is the case, we need to look at the FID and its Fourier Transform for the 20 ms point (See Figure 12),

The graph of the signal amplitude shows us the echo from the inversion recovery pulse. Though the echo is distinct from the initial pulse and FID after that pulse, we can see an overlap between that FID and the echo, which can cause an unusually high FT area for a T_I of 20 ms. To understand why there is decrease of that area till the 265 ms mark, have a look at the discussion section.

The resonant frequency used for methanol was 18.433 MHz. This was a lower resonant frequency compared to the frequencies used on the other samples since it was taken after the Easter break. The inversion times ranged from 10 ms to 3000 ms.

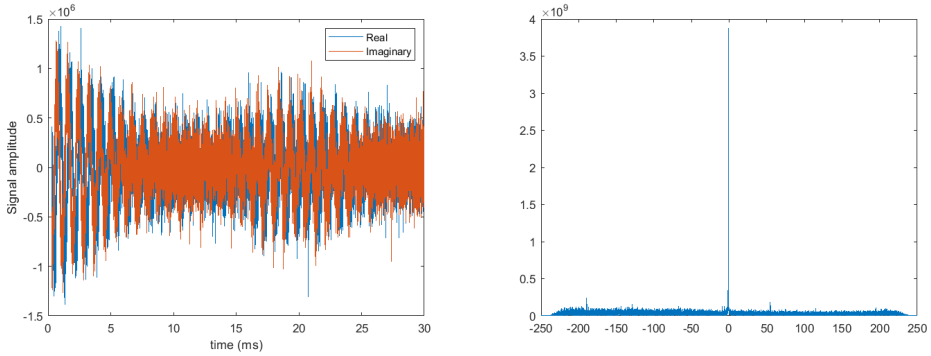

Figure 12: FID of methanol during inversion recovery and its FFT for $T_I = 20$ ms

4.1.2 Propan-1-ol

The resonant frequency used for propanol was 18.430 MHz and the inversion times ranged from 10 ms to 3000 ms. Below is the area under FT peak vs. the inversion time for propanol:

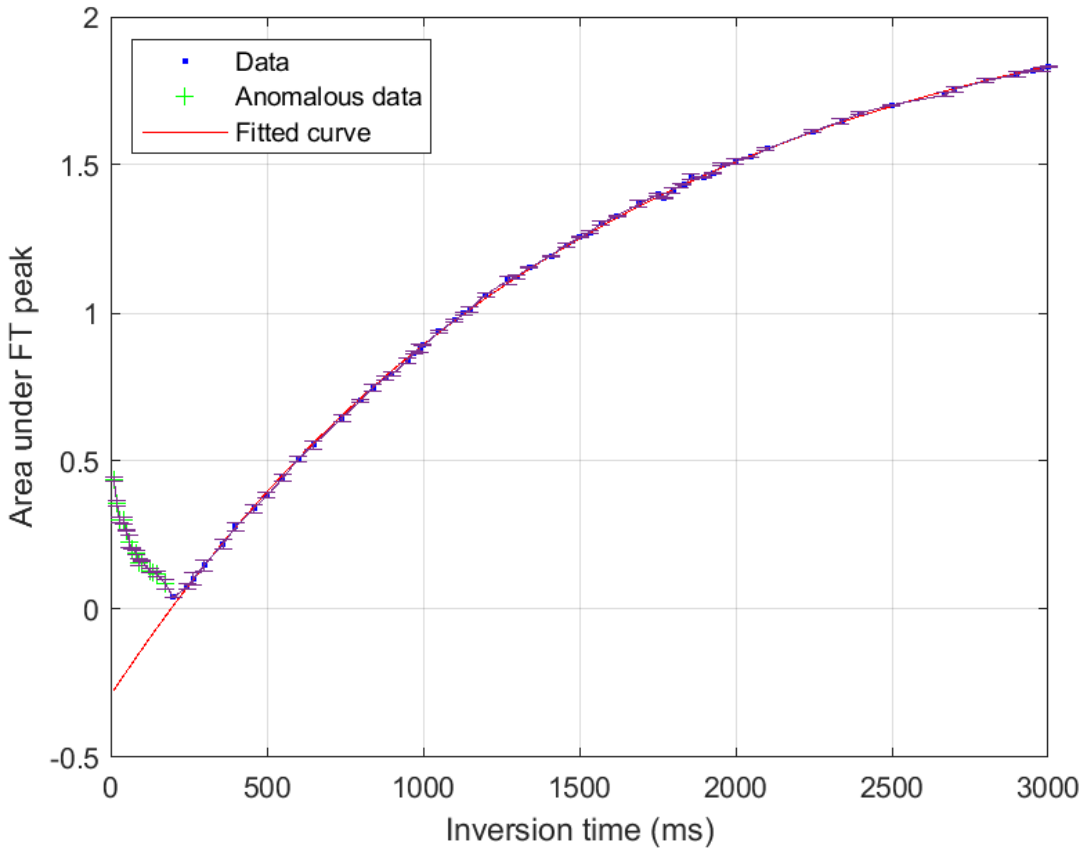

Figure 13: Area under Fourier Transform of the FID peak vs. the inversion time for propanol. The $T1$ time obtained after curve-fitting was 1541.89± 26.41 ms (95% confidence bounds) We once again see the initial dip as we saw for methanol.

4.1.3 Glycerol

The resonant frequency used for glycerol was 18.446 MHz and the inversion times ranged from 10 ms to 1000 ms. This measurement was made before the break. Below is the area under FT peak vs. the inversion time for glycerol:

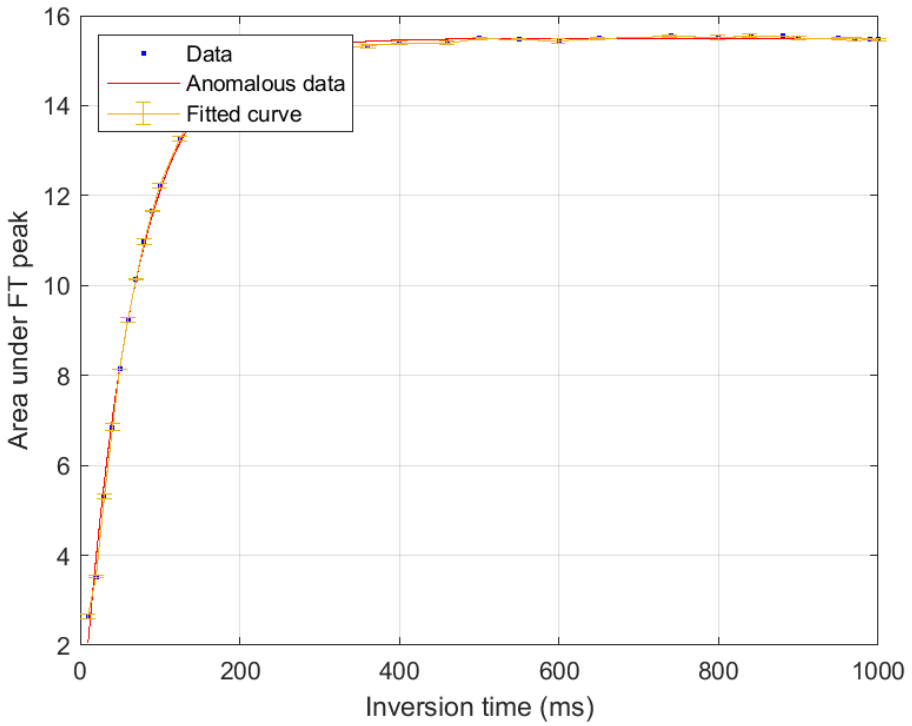

Figure 14: Area under Fourier Transform of the FID peak vs. the inversion time for glycerol. The $T1$ time obtained after curve-fitting was 65.39 ± 2.11 ms (95% confidence bounds) We don't see the same dip as seen before, however the curve is a lot more steep, giving us the lowest $T1$ value out of all the samples tested.

Glycerol and propanol have the same carbon chain length, however their $T1$ values are drastically different. This is due to their structure - particularly glycerol's CH_2 groups and propanol's CH_3 groups. We will discuss this further in the discussion section.

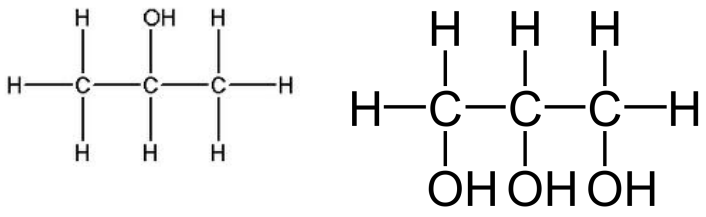

Figure 15: Molecular structures of propanol (left) and glycerol (right). Although both alcohols share the same carbon length, propanol has CH_3 groups at its ends, whereas glycerol has CH_2 groups at its ends, leading to the drastic difference in its $T1$ times.

4.1.4 Butan-1-ol

The resonant frequency used for butan-1-ol was 18.445 MHz and the inversion times ranged from 10 ms to 1000 ms. Below is the area under FT peak vs. the inversion time for butanol:

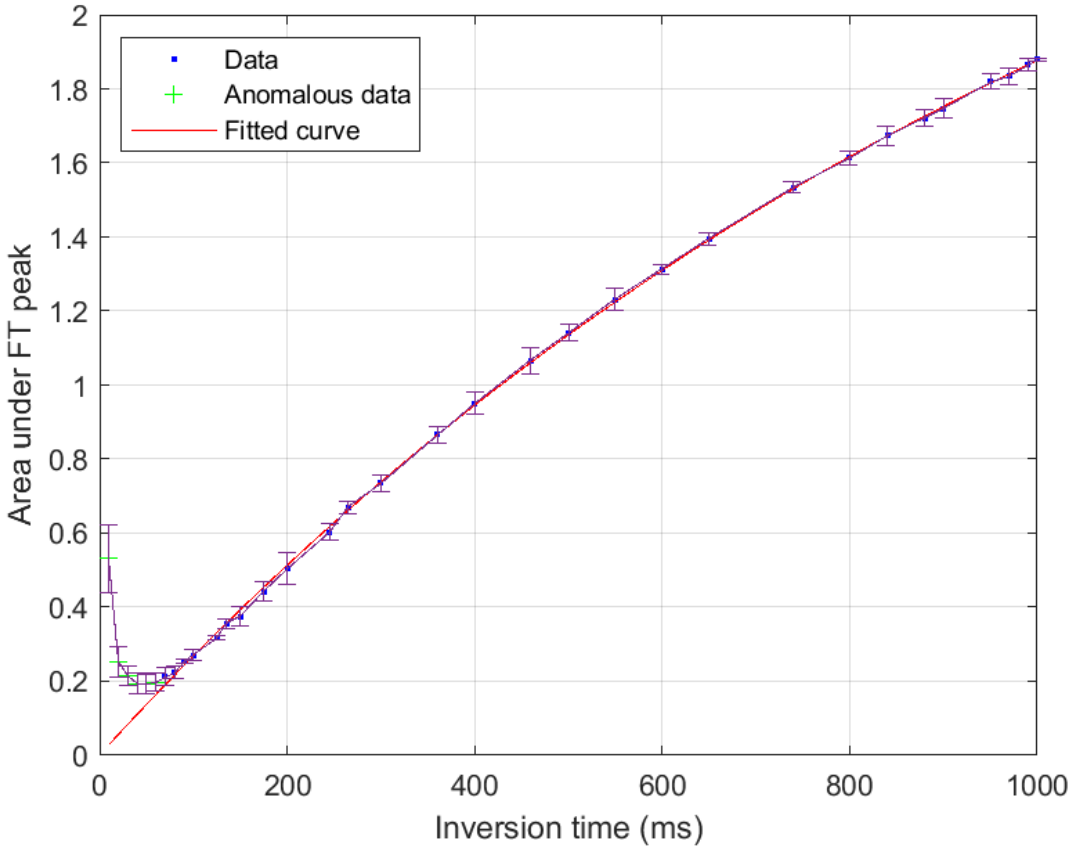

Figure 16: Area under Fourier Transform of the FID peak vs. the inversion time for butan-1-ol. The $T1$ time obtained after curve-fitting was 1176.05 $\pm$ 72.06 ms (95% confidence bounds) We see the same dip as seen before in the initial inversion times.

4.1.5 Pentan-3-ol

The resonant frequency used for pentanol was 18.4445 MHz and the inversion times ranged from 10 ms to 1000 ms. Below is the area under FT peak vs. the inversion time for pentanol (Figure 17)

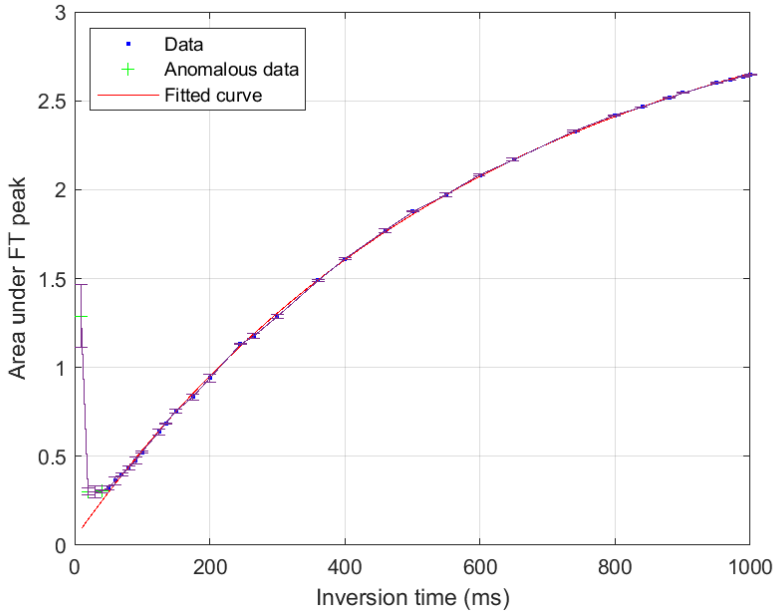

Figure 17: Area under Fourier Transform of the FID peak vs. the inversion time for pentan-3-ol. The $T1$ time obtained after curve-fitting was 602.5 ± 16.8 ms (95% confidence bounds)

4.1.6 Decan-1-ol

The resonant frequency used for decanol was 18.445 MHz. Below is the area under FT peak vs. the inversion time for decanol (Figure 18).

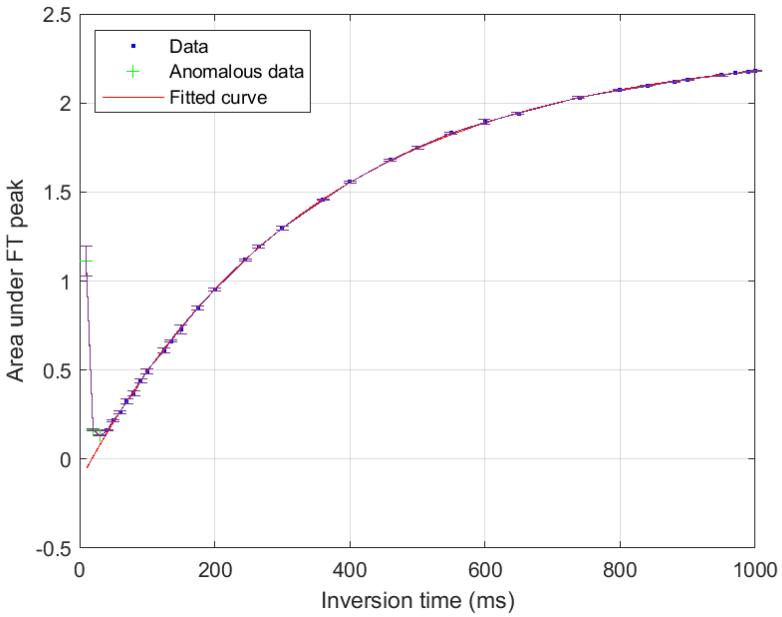

Figure 18: Area under Fourier Transform of the FID peak vs. the inversion time for decan-1-ol. The $T1$ time obtained after curve-fitting was 342.5 ± 4.2 ms (95% confidence bounds)

4.1.7 Compilation of $T1$ data for all samples

Below you can find the scaled $T1$ curves for all the samples from 10 ms to 1000 ms. There is no fitting here, but you can see the difference between the behaviours of glycerol and all the other alcohols during inversion recovery.

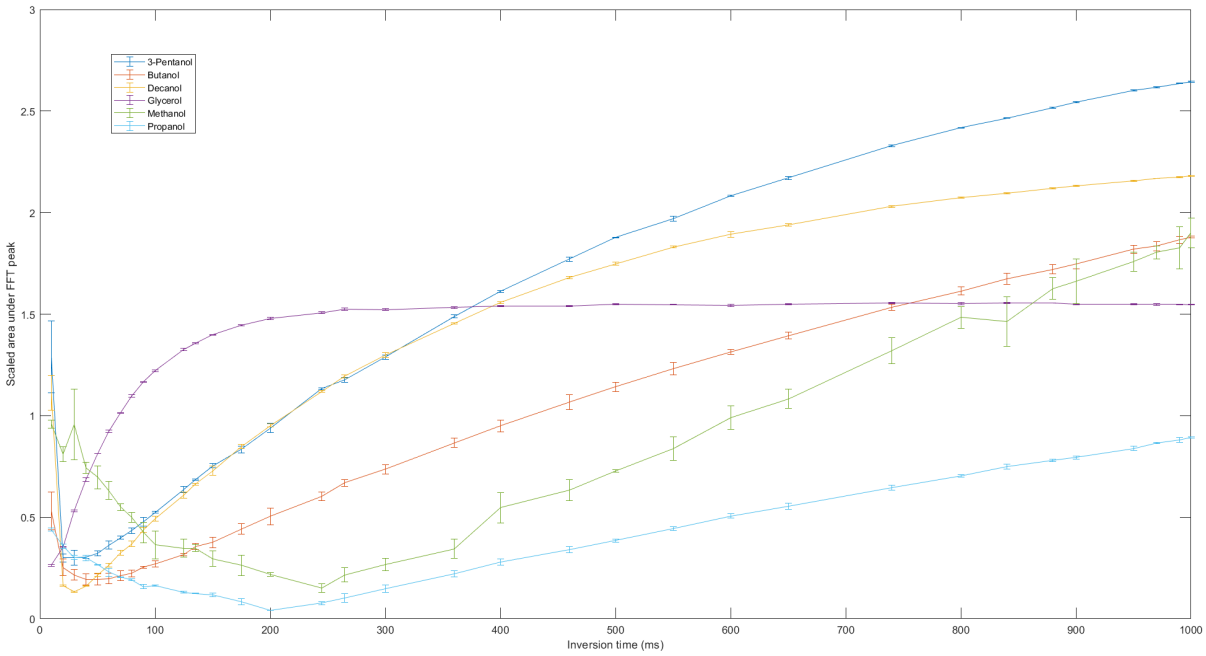

Figure 19: Scaled area under Fourier Transform of the FID peak vs. the inversion time for all samples with a range from 10 ms to 1000 ms.)

Here is a table of the alcohol samples and their $T1$ times (rounded to the nearest integer):

Sample	$T1 \pm \delta\ T1$ **ms**
Methanol	2460 ± 150
propanol	1542 ± 26
Glycerol	65 ± 2
Butan-1-ol	1176 ± 72
Pentan-3-ol	603 ± 17
Decan-1-ol	343 ± 4

Table 1: Table of alcohol samples and their $T1$ values. The errors were calculated using the 95% confidence bounds from the curve-fitting and then rounded to the nearest integer.

Using the $T1$ times, I also made a plot of $T1$ vs. the carbon chain length (See Figure 20). From the graph, we can see that as the carbon chain increases, $T1$ decreases exponentially. So we can predict that longer alcohol chains will have very short $T1$ times. Moreover, we can see the drastic drop in the $T1$ time for glycerol, which we discussed could arise form its molecular structure. We will explore more on this in the Discussion section.

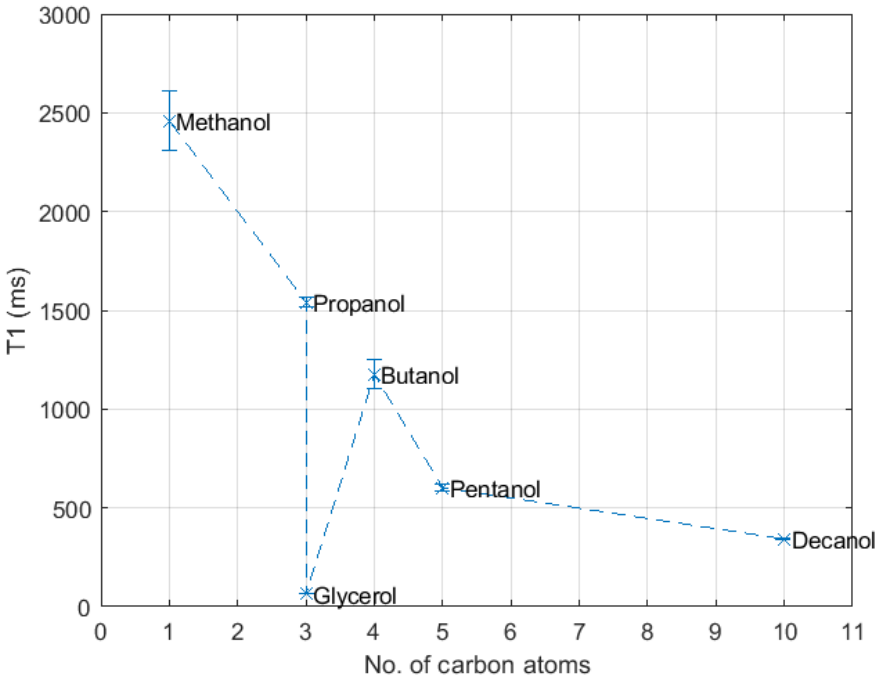

Figure 20: $T1$ time vs. carbon chain length)

4.2 $T2$

For my spin echo measurements, I used a measurement window of 15 ms for glycerol and pentanol, and 20 ms for the rest of the samples. The MATLAB program took the FFT of the echo part of the spin-echo data for all the readings. The reason for switching to a larger measurement window for the other samples was because we noticed that some of the echoes were not centred during 10 ms window, causing a shift in the FFT for that data which led to a large standard deviation in the measurements.The general fitting function used for this set of data was

$$a \exp(-x/b) + c \tag{11}$$

The fitted value of b yielded our $T2$ value for the sample.

4.2.1 Methanol

The resonant frequency used for methanol was 18.433 MHz. Below is the area under FT peak vs. the echo time for methanol.

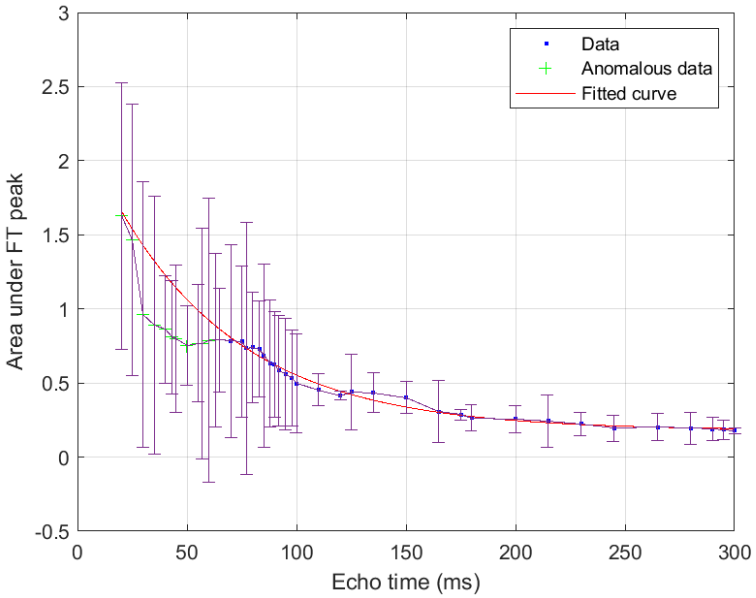

Figure 21: Area under Fourier Transform of the FID peak vs. the echo time for methanol. The $T2$ time obtained after curve-fitting was 57.99 $\pm$ 9.56 ms (95% confidence bounds)

From the graph we can see that the first few values till the 70 ms point were omitted as anomalous for the fitted curve. There were very large errors in the initial values even after repeating the experiment again on the sample. Here is the plot without error bars to see which data was omitted.

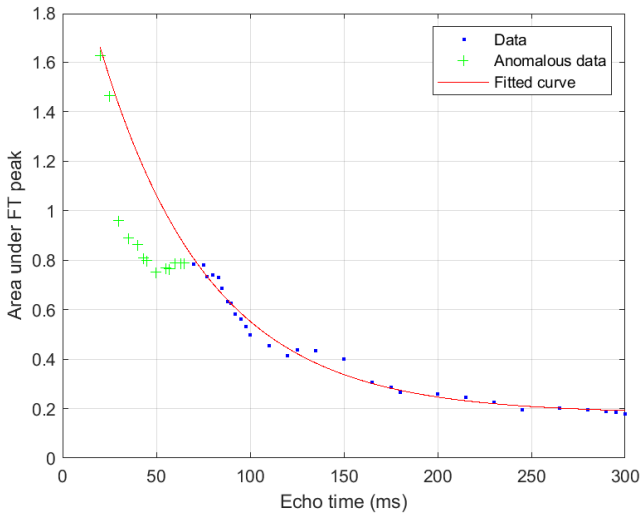

Figure 22: Area under Fourier Transform of the FID peak vs. the echo time for methanol without error bars. Points till $T_E = 70$ ms were considered anomalous due to the high error bars.

4.2.2 Propan-1-ol

The resonant frequency used for propanol was 18.430 MHz. Below is the area under FT peak vs. the inversion time for propanol:

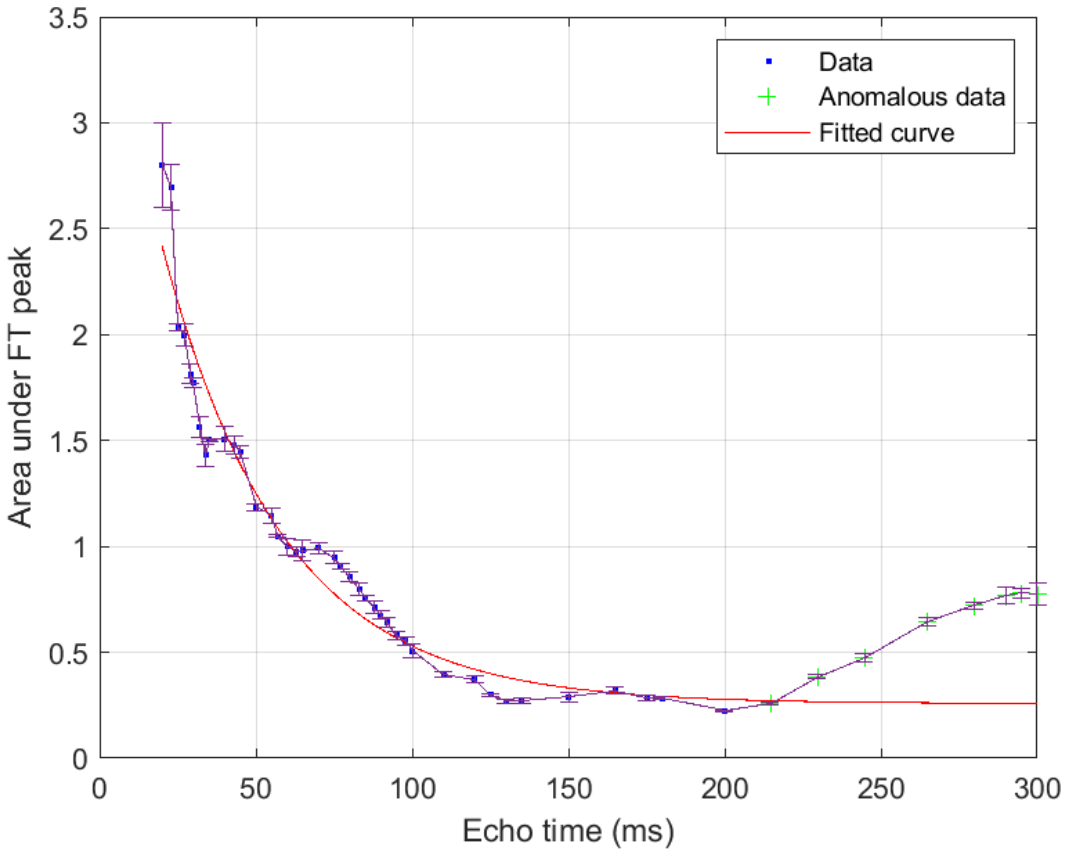

Figure 23: Area under Fourier Transform of the FID peak vs. the echo time for propanol. The $T2$ time obtained after curve-fitting was 38.60 $\pm$ 8.13 ms (95% confidence bounds)

I omitted the last few pieces of data from 210 ms to 300 ms. During the experiment, I decided to take more measurements towards the tail of the curve, but from the curve we can see that it is spurious. Also, the initial values have higher error bars - this could be due to the overlap between the echo and the FID as we saw earlier with the inversion recovery experiment.

4.2.3 Glycerol

The resonant frequency used for glycerol was 18.446 MHz. Below is the area under FT peak vs. the inversion time for glycerol. We see quite a very good exponential curve, unlike the other pieces of data. However, propanol and glycerol share very similar $T2$ values.

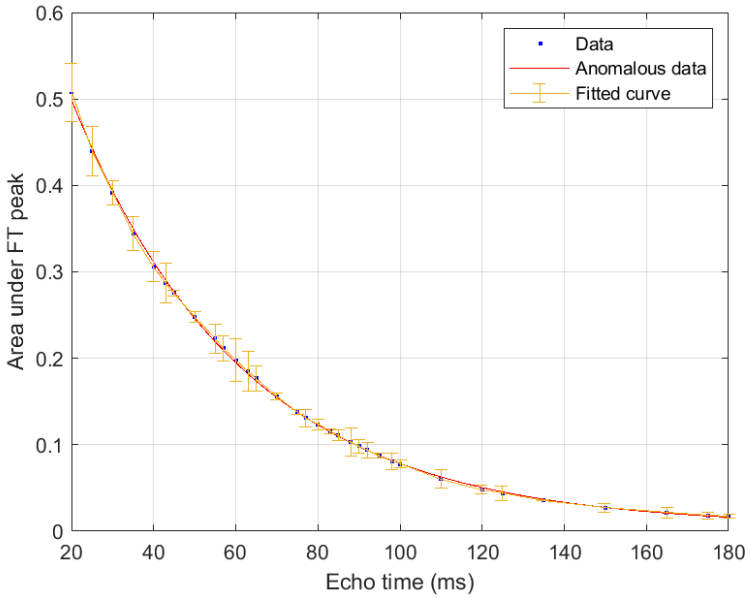

Figure 24: Area under Fourier Transform of the FID peak vs. the echo time for glycerol. The $T2$ time obtained after curve-fitting was 41.78 $\pm$ 0.88 ms (95% confidence bounds)

4.2.4 Butan-1-ol

The resonant frequency used for butanol was 18.433 MHz and the inversion times ranged from 10 ms to 1000 ms. Below is the area under FT peak vs. the inversion time for butanol:

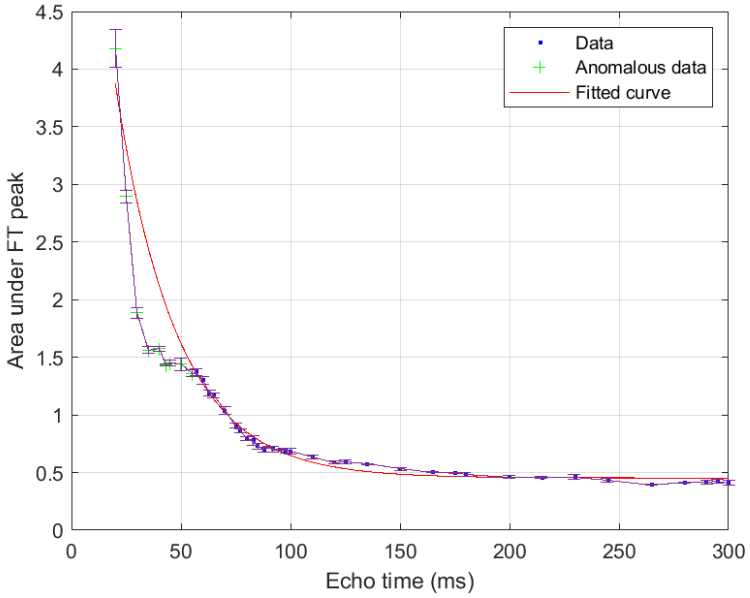

Figure 25: Area under Fourier Transform of the FID peak vs. the echo time for butan-1-ol. The $T2$ time obtained after curve-fitting was 27.91 $\pm$ 2.72 ms (95% confidence bounds).The first data points till $T_E = 55$ ms were considered anomalous.

4.2.5 Pentan-3-ol

The resonant frequency used for pentanol was 18.445 MHz and the inversion times ranged from 10 ms to 1000 ms. Below is the area under FT peak vs. the inversion time for pentanol (Figure 17)

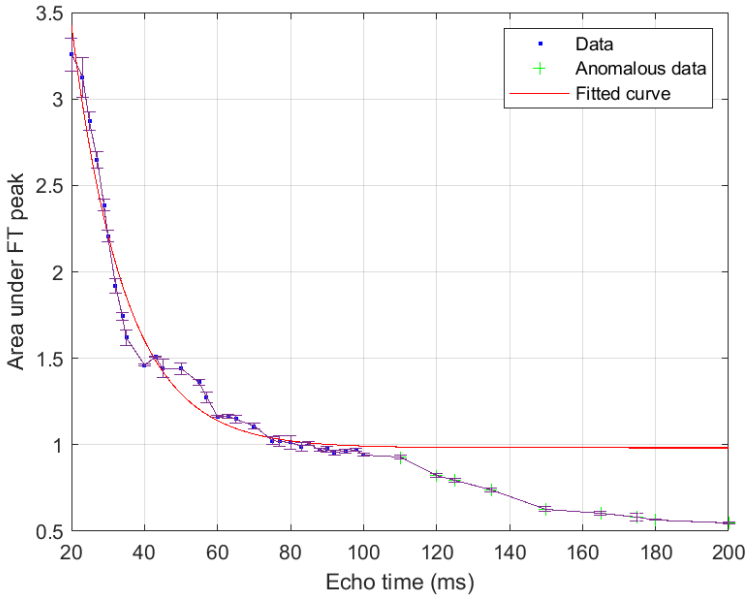

Figure 26: Area under Fourier Transform of the FID peak vs. the echo time for pentan-3-ol. The $T2$ time obtained after curve-fitting was 14.6 ± 2.0 ms (95% confidence bounds). The latter points after 100 ms were considered anomalous.

4.2.6 Decan-1-ol

The resonant frequency used for decanol was 18.43 MHz. Below is the area under FT peak vs. the inversion time for decanol (Figure 18).

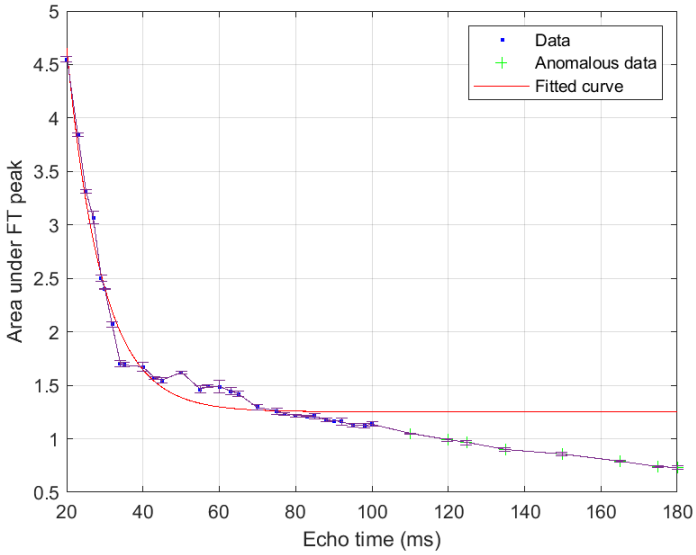

Figure 27: Area under Fourier Transform of the FID peak vs. the echo time for decan-1-ol. The $T2$ time obtained after curve-fitting was 9.3 ± 1.0 ms (95% confidence bounds). Once again, The latter points after 100 ms were considered anomalous.

4.2.7 Compilation of $T2$ data for all samples

Below you can find the scaled $T2$ curves for all the samples from 20 ms to 180 ms. There is no fitting here, but you can once again see the difference between the behaviours of glycerol and all the other alcohols during the spin echo pulse. The $T1$ curve of glycerol is a lot more smoother compared to the other alcohols.

Here is a table of the alcohol samples and their $T2$ times (rounded to the nearest integer):

Sample	$T2 \pm \delta\ T2$ **ms**
Methanol	58 ± 10
propanol	39 ± 8
Glycerol	42 ± 1
Butan-1-ol	28 ± 3
Pentan-3-ol	15 ± 2
Decan-1-ol	9 ± 1

Table 2: Table of alcohol samples and their $T2$ values. The errors were calculated using the 95% confidence bounds from the curve-fitting and then rounded to the nearest integer.

Using the $T2$ times, I also made a plot of $T2$ vs. the carbon chain length (See Figure 20). From the graph, once again we can see that as the carbon chain increases, $T2$ decreases exponentially. So we can predict that longer alcohol chains will have very short $T2$ times, similar to the prediction for $T1$. This shows us that $T2$ relaxation processes accompanies $T1$ relaxation processes. However, there lie a few exceptions - such as glycerol for this experiment.

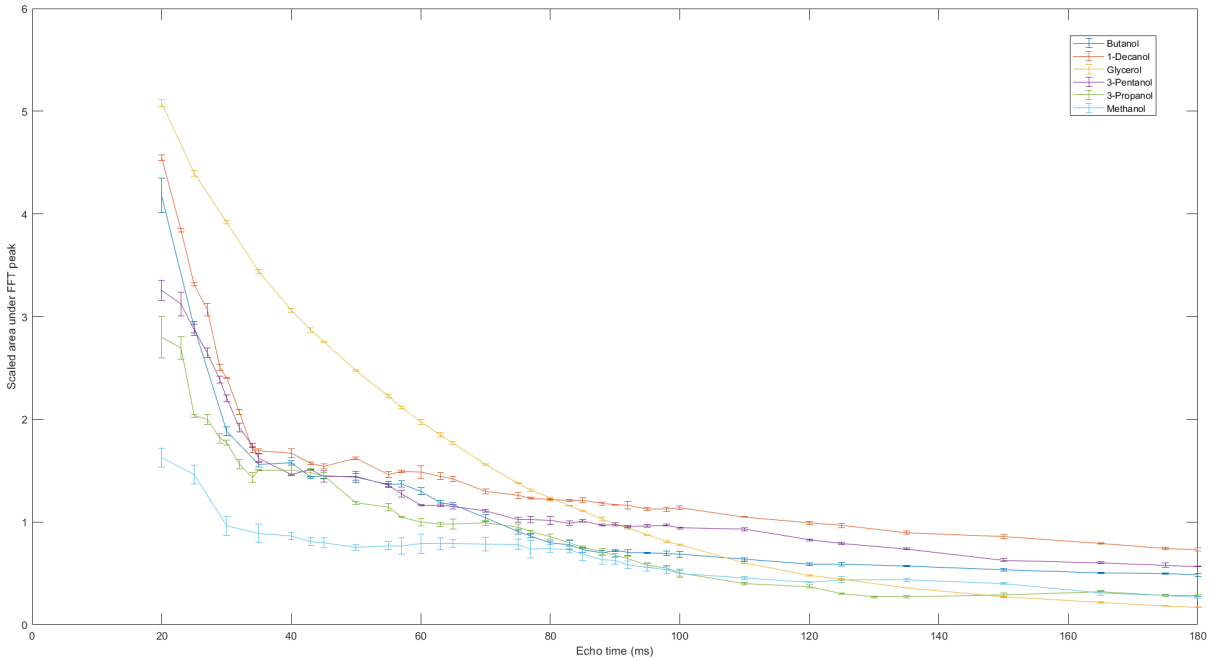

Figure 28: Scaled area under Fourier Transform of the FID peak vs. the echo time for all samples with a range from 20 ms to 180 ms.)

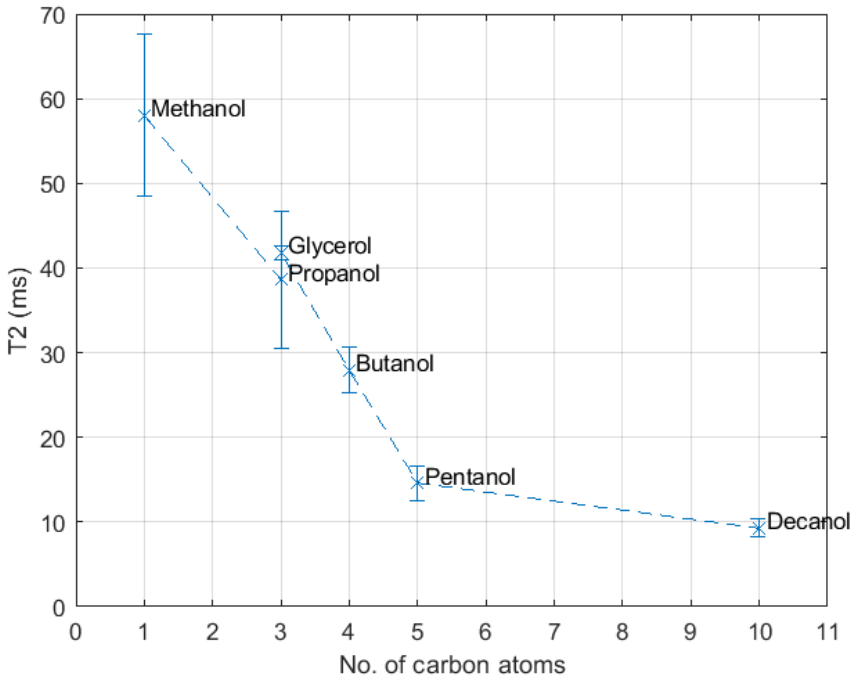

Figure 29: $T2$ time vs. carbon chain length.

5 Discussion

5.1 Decreasing FFT peak area for initial T_I values

For all our alcohols except glycerol, we saw an initial decrease of the area under the FFT peak. We know that this area directly correlates to the population of spins aligned together. Below is a zoomed in graph of the FFT at 20 ms and 100 ms for methanol:

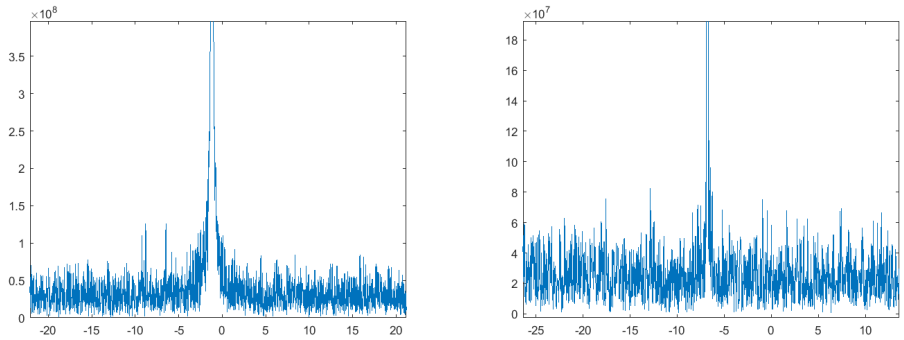

Figure 30: Zoomed in FFT of methanol at $T_I = 20$ ms (left) and $T_I = 100$ ms (right)

We see here that peak for $T_I = 100$ ms is a lot narrower, which means there are less spins aligned in the $z - axis$. This makes sense, since for really short T_I (for methanol that is till 265 ms), we would expect the population of spins to decrease as there is not a lot of time for the spins to dephase at the beginning and so they quickly come back in phase to create the echo. Therefore as T_I increases till the end of the 'dip' in the graph, we see fewer spins come into phase. Thus, the data till the 265 ms mark for methanol (and respectively for the other alcohols) does not represent $T1$ relaxation, but just the spins coming into phase. I believe that this is not an anomaly as we have seen this effect being reproduced in the other alcohols.

5.2 Glycerol and $T1$

To understand why glycerol gave us a short $T1$ time and why we didn't see an initial 'dip', we need to first introduce the concept of the **correlation time**. The **correlation time**, τ_c, is the average time it takes for a molecule to end up at an orientation 1 radian away from its starting position[5]. It is also known as the molecular tumbling rate (which is a much better name!). $T1$ is the shortest when τ_c is approximately equal to the Larmor frequency, ω. From this, we can see that CH_2 groups precess nearer to ω than CH_3 groups, as CH_2 has one less ^1H nucleus. This is what causes the very low $T1$ time for glycerol. We also see this in MRI scans - fats and oils are indicated brightly since they contain triglycerides, causing a $T1$ shortening[2].

5.3 Carbon chain length vs. $T1$ and $T2$ times

We saw earlier that as the carbon chain length increased, both $T1$ and $T2$ decreased. This could be due to the fact that as the size of the molecule increases, the molecular motion slows down below the Larmor frequency, thus creating shorter $T1$ and $T2$ times. An example of this is the short $T2$ times in solids and macromolecules. I am not entirely sure as to why the dependence between carbon chain length and $T1$ and $T2$ times looks exponential, however, in the future I can use the Stokes-Einstein relation and perhaps some molecular dynamics (MD) simulations

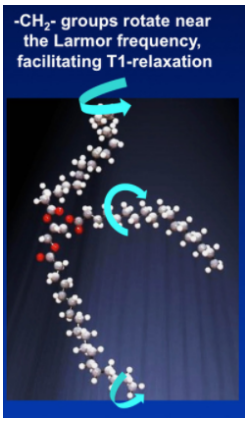

Figure 31: A triglyceride and its CH_2 groups, as seen with glycerol. Image adapted from `http://mriquestions.com/t1-bright---fat.html`

based on the correlation time and diffusion coefficient to analyse these alcohols*. Due to the time constraints and personal issues, I sadly couldn't do this analysis.

5.4 Improving the experiment

My $T1$ data was very good and in fact did not go below an R^2 value of 0.95 during curve-fitting. The same cannot be said for the $T2$ data. In the future, I can try using multiple spin-echo pulses which can increase the precision of the data. As seen mainly with methanol, the error bars in the beginning were quite large, and I believe that this can be decreased with multiple pulse sequences. Moreover, for some of the alcohols, I needed to omit the tail-end of the data as it did not follow the initial curve. I believe this can be improved if we took measurements for longer T_Es. Taking more repeats especially for the shorter alcohols did not imporve the data as the standard deviation remained almost the same. This could be due to the increased rotational motion of the alcohols, and can be remedied with the above propositions. Lastly, the cooling system used for the magnet was just a water cooler. It would be nice if we could repeat this experiment using cryogenically cooled magnets which would stablise the temperature fluctuations better than a bench-top water cooler.

6 Conclusion

Using a Red Pitaya based NMR machine, I obtained $T1$ and $T2$ values for 6 alcohol samples - methanol, propan-1-ol, glycerol, butan-1-ol, pentan-3-ol and decan-1-ol. The $T1$ times respectively were 2460 ± 150 ms, 1542 ± 26 ms, 65 ± 2 ms, 1176 ± 72 ms, 603 ± 17 ms and 343 ± 4 ms. The T2 times respectively were 58 ± 10 ms, 39 ± 8 ms, 42 ± 1 ms, 28 ± 3 ms, 15 ± 2 ms and 9 ± 1 ms. We saw that as carbon chain length increased, both $T1$ and $T2$ decreased. Glycerol had the lowest $T1$ time however, and as seen, this was due to it molecular structure instead of the carbon chain length.

*You can find some MD simulations of NMR relaxation for alkanes using the above techniques in this paper.[9]

References

[1] F. Bloch, W. W. Hansen, and Martin Packard. Nuclear induction. *Phys. Rev.*, 69:127–127, Feb 1946.

[2] E. James Delikatny, Sanjeev Chawla, Daniel-Joseph Leung, and Harish Poptani. Mr-visible lipids and the tumor microenvironment. *NMR in Biomedicine*, 24(6):592–611, 2011.

[3] Walther Gerlach and Otto Stern. Der experimentelle Nachweis der Richtungsquantelung im Magnetfeld. *Zeitschrift fur Physik*, 9(1):349–352, December 1922.

[4] E. L. Hahn. Spin echoes. *Phys. Rev.*, 80:580–594, Nov 1950.

[5] James Keeler. *Understanding NMR spectroscopy, Chapter 9 Relaxation and the NOE, Section 9.3.* Wiley, 2012.

[6] Karanjit Manak Peter Yeo. FPGA NMR Spectrometer and its Applications. "Accessed through Year 3 labs", 2019.

[7] EDWARD M. PURCELL. Research in nuclear magnetism. `http://mriquestions.com/uploads/3/4/5/7/34572113/purcell-nobel_lecture_1952.pdf`, 1952.

[8] I. I. Rabi, J. R. Zacharias, S. Millman, and P. Kusch. A new method of measuring nuclear magnetic moment. *Phys. Rev.*, 53:318–318, Feb 1938.

[9] Philip M. Singer, Dilip Asthagiri, Walter G. Chapman, and George J. Hirasaki. Molecular dynamics simulations of nmr relaxation and diffusion of bulk hydrocarbons and water. *Journal of Magnetic Resonance*, 277:15–24, 2017.